

Published in final edited form as:  
*J Am Chem Soc.* 2011 March 16; 133(10): 3390–3400. doi:10.1021/ja1072178.

## Molecular-Level Examination of Cu<sup>2+</sup> Binding Structure for Amyloid Fibrils of 40-Residue Alzheimer's $\beta$ by Solid-State NMR Spectroscopy

Sudhakar Parthasarathy<sup>1</sup>, Fei Long<sup>1</sup>, Yifat Miller<sup>2</sup>, Yiling Xiao<sup>1</sup>, Dan McElheny<sup>1</sup>, Kent Thurber<sup>4</sup>, Buyong Ma<sup>2,3</sup>, Ruth Nussinov<sup>2,5,6</sup>, and Yoshitaka Ishii<sup>\*,1</sup>

<sup>1</sup>Department of Chemistry, University of Illinois at Chicago, Chicago IL 60607

<sup>2</sup>Center for Cancer Research Nanobiology Program, NCI-Frederick, Frederick, MD 21702

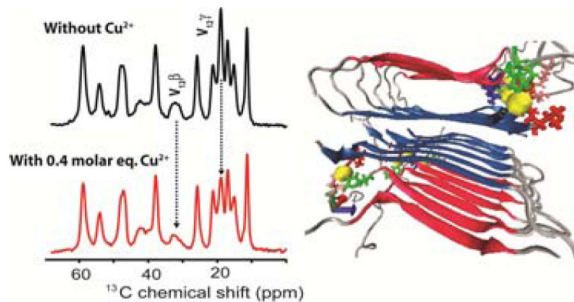
<sup>3</sup>Basic Science Program, SAIC-Frederick, Inc., NCI-Frederick, Frederick, MD 21702

<sup>4</sup>Laboratory of Chemical Physics, NIDDK, National Institutes of Health, Bethesda MD 20892

<sup>5</sup>Sackler Inst. of Molecular Medicine, Tel Aviv University, Tel Aviv 69978, Israel

<sup>6</sup>Department of Human Genetics and Molecular Medicine Sackler School of Medicine, Tel Aviv University, Tel Aviv 69978, Israel

### Abstract



Cu<sup>2+</sup> binding to Alzheimer's  $\beta$  (A $\beta$ ) peptides in amyloid fibrils has attracted broad attention, as it was shown that Cu ion concentration elevates in Alzheimer's senile plaque and such association of A $\beta$  with Cu<sup>2+</sup> triggers the production of neurotoxic reactive oxygen species (ROS) such as H<sub>2</sub>O<sub>2</sub>. However, detailed binding sites and binding structures of Cu<sup>2+</sup> to A $\beta$  are still largely unknown for A $\beta$  fibrils or other aggregates of A $\beta$ . In this work, we examined molecular details of Cu<sup>2+</sup> binding to amyloid fibrils by detecting paramagnetic signal quenching in 1D and 2D high-resolution <sup>13</sup>C SSNMR for full-length 40-residue A $\beta$ (1–40). Selective quenching observed in <sup>13</sup>C SSNMR of Cu<sup>2+</sup>-bound A $\beta$ (1–40) suggested that primary Cu<sup>2+</sup> binding sites in A $\beta$ (1–40) fibrils include N<sub>e</sub> in His-13 and His-14, and carboxyl groups in Val-40 as well as in Glu side chains (Glu-3, Glu-11, and/or Glu-22). <sup>13</sup>C chemical shift analysis demonstrated no major structural changes upon Cu<sup>2+</sup> binding in the hydrophobic core regions (residues 18–25 and 30–36). Although the ROS production via oxidation of Met-35 in the presence of Cu<sup>2+</sup> has been long suspected, our SSNMR analysis of <sup>13</sup>C<sub>e</sub>H<sub>3</sub>-S- in M35 showed little changes after Cu<sup>2+</sup> binding, excluding the possibility of Met-35 oxidation by Cu<sup>2+</sup> alone. Preliminary molecular dynamics (MD)

\*yishii@uic.edu.

**Supporting Information Available:** Details of sample preparation, Cu<sup>2+</sup> binding assays, and other SSNMR and MD data are available free of charge via the Internet at <http://pubs.acs.org/>.

simulations on Cu<sup>2+</sup>-Aβ complex in amyloid fibrils confirmed binding sites suggested by the SSNMR results and the stabilities of such bindings. The MD simulations also indicate the coexistence of a variety of Cu<sup>2+</sup>-binding modes unique in Aβ fibril, which are realized by both intra- and inter-molecular contacts and highly concentrated coordination sites due to the in-register parallel β-sheet arrangements.

## Introduction

Alzheimer's disease (AD) is characterized by the deposition of senile plaques and neural degeneration. Alzheimer's amyloid β (Aβ) peptides are a primary component of the senile plaques.<sup>1,2</sup> Among Aβ peptides ranging from 39 to 43 residues, 40-residue Aβ(1–40) and 42-residue Aβ(1–42) are the two major species found in plaque.<sup>2</sup> In AD the metal ion homeostasis appears to be severely damaged, resulting in increased concentrations of Cu and Zn ions in senile plaque, which reach 400 μM and 1 mM, respectively<sup>3</sup> or ~10 fold compared with the region outside the plaque.<sup>4,5</sup> More interestingly, it was shown that in association with Cu<sup>2+</sup>, Aβ produces reactive oxygen species (ROS) such as H<sub>2</sub>O<sub>2</sub> in vitro,<sup>6</sup> reportedly through the reduction of Cu<sup>2+</sup> to Cu<sup>+</sup> in association with M357 and/or biochemical reductants such as ascorbate.<sup>8</sup> The toxicity of Aβ can be greatly attenuated by H<sub>2</sub>O<sub>2</sub> scavengers<sup>9</sup> and metal chelator in vitro.<sup>6,10</sup> Indeed, Aβ fibrils strongly binds Cu<sup>2+</sup> ions.<sup>11–13</sup> Although the mechanisms of neural cell deaths and oxidative stress in AD are still debated, these events may be explained by the ROS generated on the redox-active Cu<sup>2+</sup> ions bound on Aβ fibrils, which was observed in vitro. Small molecules which target metal-Aβ interactions have been tested as potential therapeutic agents,<sup>14–16</sup> including one in a clinical trial.<sup>14</sup> Thus, intensive efforts have been made to understand the molecular details of Cu<sup>2+</sup>-binding to Aβ.<sup>8,17–33</sup> On the other hand, most structural studies on Cu<sup>2+</sup>-Aβ binding were performed on soluble model peptides<sup>19–24,29</sup> or monomeric Aβ<sup>25–27,33</sup>; however, some of these reports are controversial.

Solution NMR studies by Hou and Zagorski on monomeric Aβ(1–40) indicated specific binding of Cu<sup>2+</sup> to side-chains of H6, H13, and H14 by their upfield <sup>1</sup>H shifts, while suggesting the lack of association of D1 and Y10 with Cu<sup>2+</sup> through little perturbation on their <sup>1</sup>H side-chain shifts.<sup>27</sup> The Cu<sup>2+</sup> binding to the N-terminal region is consistent with a recent NMR study indicating paramagnetic relaxation enhancement on the residue 3–16 upon the addition of Cu<sup>2+</sup> to monomeric Aβ(1–40).<sup>25</sup> EPR spectra of Cu<sup>2+</sup>-bound Aβ(1–16), Aβ(1–28), and Aβ(1–42) monomers show quite similar spectral features for Cu<sup>2+</sup><sup>19–21</sup>; it has been proposed that these EPR spectra suggests the presence of two types of Cu<sup>2+</sup> binding sites, both of which are likely to have 4-coordination geometries such as 2N/2O and 3N/1O coordination to Cu<sup>2+</sup>.<sup>19–21</sup> This is consistent with the solution NMR results<sup>27</sup> since two nitrogens of His imidazole rings typically offer coordination to Cu<sup>2+</sup>.<sup>34</sup> More detailed isotope-edited EPR studies on Aβ(1–16) suggested Cu<sup>2+</sup> coordination to D1, H6, H13 (or H14) for one spectral component (Component I; A<sub>II</sub> = 162 ± 3 G and g<sub>II</sub> = 2.272) and the second Cu<sup>2+</sup> coordination to A2, H6, H13, H14 for the other minor spectral component at a neutral pH (Component II; A<sub>II</sub> = 148 ± 3 G and g<sub>II</sub> = 2.227).<sup>19,20</sup> In contrast, a recent EPR study on monomeric Aβ(1–28) suggested octahedral coordination by D1, D7, H6, H13, H14 for a EPR spectrum having similar yet distinguishable EPR parameters (Component I: A<sub>II</sub> = 170 G and g<sub>II</sub> = 2.27; Component II: A<sub>II</sub> = 156 G and g<sub>II</sub> = 2.22).<sup>21</sup> Although these Aβ monomer and fragments may have different metal binding modes, a conclusive structural model of Cu<sup>2+</sup>-Aβ complex has not been established even for the soluble model systems (see Table 1 in ref. 8 for example). More importantly, monomeric Aβ is non-toxic; a question relevant to the mechanism of AD is, therefore, Cu<sup>2+</sup> binding structure in Aβ aggregates. Recent EPR studies on Cu<sup>2+</sup>-bound amyloid fibril of Aβ(1–40) and Aβ(1–42) report the presence of, at least, two types of binding sites that also have 4-coordination

geometries.<sup>21,28,31,35</sup> However, beyond the similarity of the EPR spectra of the A $\beta$  fibrils with those of more well studied soluble A $\beta$  fragments, scarce site specific information on metal binding modes has been obtained for A $\beta$  fibrils. A recent EPR study on A $\beta$ (1–28) showed no notable changes in the EPR by H6A or H14A mutation.<sup>21</sup> Thus, similarity in conventional continuous wave (cw) EPR spectra among Cu(II)-bound A $\beta$  with varied sequences may not be sufficient to deduce Cu<sup>2+</sup> coordination structure uniquely. Rather, coordination to Cu<sup>2+</sup> involving different His residues and other ligands can yield very similar 1D EPR spectra as long as the local environments around Cu<sup>2+</sup> are similar. On Cu<sup>2+</sup> binding to oligomeric A $\beta$ , there were some interesting studies,<sup>25,35</sup> yet the nature of these oligomeric species has not been well defined. A recent study by solid-state NMR (SSNMR), a powerful method for structural analysis of protein aggregates<sup>36–46</sup> and other proteins,<sup>47–62</sup> indicated Cu<sup>2+</sup> binding to A $\beta$  in membrane environments.<sup>63</sup> Despite the broad attention and the intense efforts presented in the previous studies,<sup>8,17–25,27–29</sup> the exact Cu<sup>2+</sup> binding sites of A $\beta$  fibrils *have not been identified with any site-specificity*. Lack of site-specific structural information has also severely limited our molecular-level understanding on structural changes of A $\beta$  fibrils upon Cu<sup>2+</sup> binding. Such detailed structural information would be highly valuable for revealing still unknown mechanisms of the toxicity for A $\beta$  aggregates and designing metal binding inhibitors for amyloid aggregates.<sup>14–16</sup>

Here, we present the first systematic study to address molecular details of Cu<sup>2+</sup> binding on amyloid fibrils of full-length A $\beta$ (1–40) by SSNMR. With recent advance in SSNMR for paramagnetic proteins,<sup>45,47,64–67</sup> we examine the possibility of identifying site-specific Cu<sup>2+</sup> binding to A $\beta$ (1–40) fibrils and molecular-level structural changes upon the binding. Our SSNMR data show a lack of perturbation to <sup>13</sup>C chemical shifts by Cu<sup>2+</sup> binding, and suggest that the parallel  $\beta$ -sheet structures in the hydrophobic core regions of A $\beta$ (1–40) fibrils are not reorganized into different structures by Cu<sup>2+</sup> binding for the first time. Molecular dynamics (MD) simulations that take account of the amyloid fibril structure suggest that Cu<sup>2+</sup> binding to A $\beta$  in fibril is likely to involve the novel binding modes that are not possible in soluble fragments or monomers of A $\beta$ .

## Results and Discussion

First, we examined the morphological changes of amyloid fibril after Cu<sup>2+</sup> binding. Although it has been proposed that Cu<sup>2+</sup> or Zn<sup>2+</sup> binding to A $\beta$  monomers may modulate misfolding kinetics,<sup>27,30,35,68,69</sup> in this work, we focus on structural changes due to Cu<sup>2+</sup> binding after the fibril formation. Figures 1a and 1b show transmission electron microscopy (TEM) images of A $\beta$  fibrils without and with 0.4 mol eq CuCl<sub>2</sub>, respectively. The fibrils without Cu<sup>2+</sup> have a diameter of ~9 nm and a length of > 1  $\mu$ m, which are consistent with previous reports.<sup>70</sup> The morphology of the A $\beta$  fibrils is retained after Cu<sup>2+</sup> was bound to fibrils. Although it is difficult to deduce any molecular-level structural changes from the data, it is likely that Cu<sup>2+</sup> binding does not substantially destabilize the amyloid fibril structure. Binding of Cu<sup>2+</sup> to A $\beta$  fibrils was determined by photometric assay using N,N,N',N'-tetraethylthiuram disulfide as a Cu<sup>2+</sup> indicator.<sup>71</sup> We confirmed that more than 95% of Cu<sup>2+</sup> was bound to A $\beta$ (1–40) for both CuCl<sub>2</sub> and CuGly when the ratio of Cu<sup>2+</sup> to A $\beta$  ( $f_{Cu/A\beta}$ ) was 0.5 or less (see SI). However, at  $f_{Cu/A\beta} = 1.0$ , 5.3 % and 15 % of Cu<sup>2+</sup> ions were *not* bound to A $\beta$  fibrils for CuCl<sub>2</sub> and CuGly, respectively (see SI). Based on these results, we selected  $f_{Cu/A\beta} = 0.4$  throughout the following SSNMR study as a condition where nearly all Cu<sup>2+</sup> ions are *strongly* bound to A $\beta$  fibrils.

Next, we examined whether any site-specific binding of Cu<sup>2+</sup> can be detected by SSNMR for A $\beta$ (1–40) fibrils. Figure 1c show a comparison of the aliphatic region of 1D <sup>13</sup>C CPMAS SSNMR spectra of A $\beta$ (1–40) amyloid fibrils (black) without and (red) with 0.4 molar eq. of Cu<sup>2+</sup> to A $\beta$ . The A $\beta$ (1–40) samples were isotope labeled with uniformly <sup>13</sup>C-

and  $^{15}\text{N}$ -labeled amino acids at V12, F20, A21, I31, G33, and  $^{13}\text{C}_\epsilon$ -selectively labeled M35 (see SI). Interestingly, most sites display no significant changes in the signal intensities. This includes  $^{13}\text{C}_\epsilon$  of M35 (green arrow), which has been long suspected as the site that is responsible for the production of  $\text{H}_2\text{O}_2$  through interactions with  $\text{Cu}^{2+}$ .<sup>72,73</sup> If M35 side chain (-S-C $\epsilon$ H<sub>3</sub>) is oxidized into -SO-CH<sub>3</sub> as hypothesized previously,<sup>7</sup>  $^{13}\text{C}_\epsilon$  shift at 15.6 ppm should be altered to ~40 ppm.<sup>74</sup> However, no major changes in the signal intensity or chemical shift were observed for  $^{13}\text{C}_\epsilon$  M35 after a month. In contrast, signal intensities drop by 36% and 27% selectively for  $^{13}\text{C}_\gamma$  and  $^{13}\text{C}_\beta$  of V12 (orange arrows), respectively upon  $\text{Cu}^{2+}$  binding. The site is nearby to H13/H14, which were reported to interact with  $\text{Cu}^{2+}$  for  $\text{A}\beta(1-40)$  monomer.<sup>27</sup> These results suggest that the effect of  $\text{Cu}^{2+}$  binding to fibrils is site specific, quenching the signals for sites in the vicinity of  $\text{Cu}^{2+}$  (V12 in this case). In a recent SSNMR study of Cu, Zn SOD, signal quenching of  $^{13}\text{C}$  within a ~5 Å radius of  $\text{Cu}^{2+}$  was reported.<sup>47</sup> Here, we utilize such paramagnetic quenching to identify  $\text{Cu}^{2+}$  binding sites in the aggregated form of the  $\text{A}\beta$  proteins.

Figure 1d shows a comparison of 2D  $^{13}\text{C}/^{13}\text{C}$  spectra of the same  $\text{A}\beta$  fibril samples (black) without and (red) with  $\text{Cu}^{2+}$  bound to  $\text{A}\beta$  in a superposition. Most of the signals are well resolved without signal overlap. Remarkably, the  $\text{Cu}^{2+}$ -bound fibril have nearly identical chemical shift positions (within  $\pm 0.2$  ppm) and intensities with those for the  $\text{Cu}^{2+}$ -free fibril, except for the V12 signals (orange arrows). Since  $^{13}\text{C}$  chemical shifts are a probe very sensitive to protein conformations, this presents interesting evidence that the site-specific  $\text{Cu}^{2+}$  binding does not alter the conformations of  $\text{A}\beta$  in the  $\beta$ -sheet cores, including F20, A21, I31. Additional results below support this finding. Thus, we concluded that  $\text{Cu}^{2+}$ -binding does not introduce major conformation changes except for the N- and C-terminal regions, where binding is likely to take place, as will be discussed.

Based on the above results, we hypothesized that  $\text{Cu}^{2+}$  ions are interacting with H13 and H14 side chains in the  $\text{A}\beta$  fibril, and with other neighboring residues. To test this, we performed  $^{13}\text{C}$  SSNMR of  $\text{A}\beta(1-40)$  fibril samples in which one of these residues was uniformly  $^{13}\text{C}$ -labeled. Figures 2a,b show 1D  $^{13}\text{C}$  CPMAS spectra of (a) H13 and (b) H14 side chains for  $\text{A}\beta$  fibrils (black) without and (red) with  $\text{Cu}^{2+}$  bound to  $\text{A}\beta$ , together with signal assignments. Clearly, the signals for both H13 and H14 are quenched considerably by  $\text{Cu}^{2+}$ . Spectral analysis of the aromatic side chains shows that signals for  $^{13}\text{C}_\delta$  and  $^{13}\text{C}_\epsilon$  in H13/H14 are quenched by 30–60%, while those for  $\text{C}_\gamma$  are quenched less (by ~15%). This suggests that  $\text{Cu}^{2+}$  ion favors coordination to N $\epsilon$  in H13 and H14, which is one bond away from  $^{13}\text{C}_\delta$  and  $^{13}\text{C}_\epsilon$ , over that to N $\delta$ . As a control, we examined paramagnetic quenching for F20 (Figure 2c), which shows nearly no quenching. Previous studies indicated the involvement of N $\delta$ /N $\epsilon$  of histidine in  $\text{A}\beta(1-40)$  in  $\text{Cu}^{2+}$  binding.<sup>26,27,75</sup> Raman spectroscopic studies<sup>26</sup> shows that  $\text{A}\beta(1-40)$  precipitates obtained by the addition of  $\text{Cu}^{2+}$  to a  $\text{A}\beta$  solution display  $\text{Cu}^{2+}$  coordination to N $\epsilon$ , in His while  $\text{A}\beta(1-40)$  monomers in a solution show  $\text{Cu}^{2+}$  coordination to N $\delta$  at pH 7.4. Barnham *et al.*<sup>75</sup> reported that  $\text{A}\beta(1-40)$  having N-methylated His for N $\epsilon$  at position His 6,13 and 14 has weaker metal-ligand interaction than WT  $\text{A}\beta$  or  $\text{A}\beta(1-40)$  having N-methylated His for N $\delta$ . The results are consistent with our finding. To the best of our knowledge, this is the first experimental data that directly demonstrate the association of  $\text{Cu}^{2+}$  with H13 and H14 of  $\text{A}\beta(1-40)$  in amyloid fibrils with site resolution.

Figure 2d shows the summary of the residues quenched by  $\text{Cu}^{2+}$  binding for 6  $\text{A}\beta$  samples selectively isotope labeled at different sites (see SI). Only a limited number of aliphatic side chains were quenched by  $\text{Cu}^{2+}$  bound to  $\text{A}\beta$  (see Figure S2 in SI). Apart from the significant changes in the N-terminal region, V24, and V39, other sites in the residues 17–38 show very limited perturbation from  $\text{Cu}^{2+}$  on the signal intensities. Similar signal quenching profile was obtained for  $\text{A}\beta(1-40)$  fibrils prepared at Dr. Tycko's lab at the NIH without

agitation<sup>70,76</sup> (see SI and Figure S3). Importantly, we also found that <sup>13</sup>C chemical shifts are not altered upon Cu<sup>2+</sup> binding by more than 0.2 ppm for the hydrophobic core regions (residues 18–25 and 30–36) except for the moderate perturbation (~0.35 ppm) on some sites of F19 and G33 (Table S1). The results provide the first crucial experimental evidence that Cu<sup>2+</sup> binding does not reorganize or alter the parallel  $\beta$ -sheet structures of the hydrophobic core regions for A $\beta$ (1–40) fibril with site resolution.

To identify other binding sites, we further performed 2D <sup>13</sup>C/<sup>13</sup>C correlation SSNMR (Figure 3a) of uniformly <sup>13</sup>C- and <sup>15</sup>N-labeled A $\beta$ (1–40) fibrils (black) without and (red) with Cu<sup>2+</sup>. Surprisingly, as shown in the slices (Figure 3b–d), considerable signal quenching by 45±11 % and 59±9 % due to Cu<sup>2+</sup> (orange arrows) was observed for <sup>13</sup>CO<sub>2</sub><sup>−</sup> of (d) V40 in the C-terminus and (b) Glu side chains, respectively. The extent of the quenching due to Cu<sup>2+</sup> is comparable to those for His-13 and His-14. Although Glu signals were not assigned to individual residues, the results clearly suggest Cu<sup>2+</sup> bindings to the carboxyl terminus of V40 and side chains of Glu. Whereas binding to Glu was hypothesized in previous studies,<sup>8</sup> such Cu<sup>2+</sup> binding, including that to the C-terminus, has been difficult to examine for A $\beta$  fibrils until this work. Although site directed mutations may be effective for short A $\beta$  fragments,<sup>29</sup> such mutations on the full-length A $\beta$  may alter the structure of amyloid fibril. The data in Figure 3a also indicate signals for other side-chain carboxyl groups at 175–180 ppm are likely quenched by Cu<sup>2+</sup> binding; further studies will be needed for signal assignments and detailed analysis. With these SSNMR results, we conclude that the N-terminal region including H13, H14, and Glu side chains and the CO<sub>2</sub><sup>−</sup> in the C-terminus are highly likely to play major roles in Cu<sup>2+</sup> binding to the A $\beta$ (1–40) fibril. The Cu<sup>2+</sup> binding is likely to make very little or no changes on the basic structural units in the hydrophobic cores of the A $\beta$  amyloid fibril.

To elucidate possible Cu<sup>2+</sup> binding structures to A $\beta$ , we performed two sets of MD simulations of A $\beta$ (1–40) fibrils with Cu<sup>2+</sup>. As the initial structure, we adopted a structural model from Tycko's group<sup>77</sup> with a fixed geometry for the residues 15–39 for oligomeric A $\beta$ . In the first set of the MD simulation, we used cationic dummy atom (CaDa) approach for Cu<sup>2+</sup> ions in order to identify possible Cu<sup>2+</sup> binding ligands.<sup>78</sup> Based on our SSNMR results, Cu<sup>2+</sup> ions were non-covalently bound to N<sub>e</sub> of H13 (or H14 in Figure 5) by ionic interactions in the initial structure. Indeed, the final structure with implicit solvents after three thermal annealing cycles demonstrated that CO<sup>2−</sup>/CO side chains of D1, E3, E11, Q15, and the CO<sup>2−</sup> terminal of V40 coordinate to Cu<sup>2+</sup>, despite the absence of such interactions in the initial structures (Figure 4). While previous EPR studies for monomeric A $\beta$  fragments<sup>8,19,20,27</sup> predicted two major coordination modes, here we suggest that a variety of coordination structures are likely to coexist in the amyloid fibril. Many of these observed binding modes are realized by the parallel  $\beta$ -sheet arrangements, in which Cu<sup>2+</sup>-coordination sites at the N-terminal are concentrated via aggregation. For example, some Cu<sup>2+</sup> ions were bridged by two H13 (or H14) rings of each two peptides (orange circles in Figure 4a and Figure 5a). Such binding mode is not possible in a monomer, although the possibility of Cu<sup>2+</sup>-mediated inter-molecular His bridge was proposed for an A $\beta$  dimer previously.<sup>69</sup> Also, the Cu<sup>2+</sup> ions bridge carboxyl terminal of V40 and H13 (or E11); such a binding has not been reported for monomeric A $\beta$ . It should be noted that the above MD simulation results do not necessarily exclude the previously proposed coordination models by EPR and other studies. Our SSNMR results indeed indicate substantial relaxation on F4, which is consistent with the Cu<sup>2+</sup> coordination to H6, which was proposed by the previous EPR and NMR studies.<sup>19,27,28</sup> In our preliminary MD simulations in Fig. 4–5, such long-range coordination may not be completely reproduced probably because of the restricted time frame of the simulations (20 ns) and the limited ensemble of the initial structures. Our MD simulation starting from a different initial structure with some Cu<sup>2+</sup> ions coordinated to N<sub>e</sub> of H6, H13, H14 showed that a common Cu<sup>2+</sup> ion can be coordinated to H6 and H14 of

$\text{A}\beta$  fibril (data not shown). It is possible that the various unique coordination modes presented here for the amyloid fibril coexist with those proposed for the monomeric/fragment  $\text{A}\beta$  at different population and perhaps in a dynamically exchangeable manner.<sup>27</sup>

To confirm the presence of various coordination modes, we examined the stability and the conformational energies for  $\text{A}\beta(1\text{--}40)$  fibril models of three different  $\text{Cu}^{2+}$ -binding modes (Table 1, Figure 6) with a more elaborate MD simulations using explicit solvents based on a recent study on  $\text{Zn}^{2+}\text{-A}\beta$  oligomer association.<sup>68</sup> The simulations show that such  $\text{Cu}^{2+}$ -coordination modes are all stable over 20 ns. In Conformer 1,  $\text{Cu}^{2+}$  binds to His-6, His-13 and His-14 (Fig. 6a) and in Conformer 2,  $\text{Cu}^{2+}$  binds to Asp-1, His-6 and His-14 (Fig. 6b). As shown in Table 1, Conformer 1 (Fig. 6a) is more stable than Conformer 2 (Fig. 6b); this indicates that the interaction of  $\text{Cu}^{2+}$  with His is likely to stabilize the model more than Asp, although the energy difference is within standard deviation due to thermal fluctuation. In Conformer 3, 4  $\text{Cu}^{2+}$  ions interact with D1, H6 and H14 and 4  $\text{Cu}^{2+}$  ions bind to D1, H14 and V40 (Fig. 6c); in Conformer 4, the latter set of ligands are D1, H13 and V40 (Fig. 6d). Conformer 4, which has  $\text{Cu}^{2+}$  coordination to  $-\text{CO}_2^-$  of V40 and side chains of D1 and H13, shows higher stability than Conformer 2. The coordination of  $\text{Cu}^{2+}$  to D1, H14, V40 in Conformer 3, also has a slightly higher stability than that of D1, H6 and H14 in Conformer 2. These results suggest that  $\text{Cu}^{2+}$  may indeed interact with the C-termini, as suggested by our SSNMR analysis.

The simulations presented here are intended to provide insights into the possible ligands coordinated to  $\text{Cu}^{2+}$  in the  $\text{A}\beta$  amyloid fibril. At this point, universal force fields are not available for MD simulations involving  $\text{Cu}^{2+}$  ions.<sup>18,79,80</sup> Development of more optimized force fields is likely needed to reproduce more accurate coordination geometries for detailed comparison with EPR spectra. Despite the limitation, the MD simulation results allowed for the evaluation of  $\text{Cu}^{2+}$  coordination modes for more realistic  $\text{Cu}^{2+}\text{-A}\beta$  fibril model based on our SSNMR results, which suggested that the structural changes by  $\text{Cu}^{2+}$  binding are restricted to the N-term and C-term regions. It is encouraging that the two separate sets of MD simulations both suggested the previously unexpected unique coordination modes that are consistent with our SSNMR relaxation data.

In conclusion, this study has presented molecular details of  $\text{Cu}^{2+}$ -bound  $\text{A}\beta(1\text{--}40)$  amyloid fibril system by SSNMR. Three chemically and biologically novel aspects are presented in our work. First, this study has demonstrated the first systematic approach to examine binding of  $\text{Cu}^{2+}$  to insoluble amyloid aggregates at site specific level by SSNMR, based on the recent progress in SSNMR for small paramagnetic compounds<sup>66,81–84</sup> and for paramagnetic proteins<sup>45,47,49,67</sup> by our groups and other. We have shown that uses of paramagnetic quenching and chemical-shift perturbation in SSNMR can be effectively employed in order to examine possible  $\text{Cu}^{2+}$  binding sites and structural changes upon  $\text{Cu}^{2+}$  binding for insoluble amyloid system. Second, this study has, for the first time, provided detailed site-specific structural information on  $\text{Cu}^{2+}$  bound full-length  $\text{A}\beta(1\text{--}40)$  in amyloid fibrils. Despite the linkage of the  $\text{Cu}^{2+}\text{-A}\beta$  fibril with AD and its significance as a potential pharmaceutical target,<sup>14–16</sup>  $\text{Cu}^{2+}\text{-A}\beta$  association has been examined mostly for smaller and early-stage model systems such as soluble  $\text{A}\beta$  fragments or  $\text{A}\beta$  monomers. Our study has offered a solution to this situation by overcoming the difficulties in the sample preparation and the lack of suitable structural analysis methods for  $\text{Cu}^{2+}\text{-A}\beta$  in amyloid fibrils, for which structural information has been very scarce. Third, our SSNMR data experimentally demonstrated various novel features of  $\text{Cu}^{2+}$  coordination to the  $\text{A}\beta$  fibril. Besides offering experimental evidence of the  $\text{Cu}^{2+}$  coordination to  $\text{N}_e$  of H13 and H14, this study has revealed previously unexpected ligands such as the carboxyl group of V40 at the C-terminus and Glu side chains. Our chemical-shift perturbation data suggested very little structural changes for the hydrophobic core regions (residues 18–25 and 30–36) of the  $\text{A}\beta$  fibrils upon

$\text{Cu}^{2+}$  binding. The unique coordination modes suggested by SSNMR were confirmed by the two sets of MD simulations on sophisticated  $\text{A}\beta$  oligomer models reflecting realistic amyloid fibril structures. Unlike previous MD studies on  $\text{Cu}^{2+}$ - $\text{A}\beta$  binding,<sup>18</sup> both MD simulations incorporated intermolecular parallel  $\beta$ -sheet structure that is characteristic of the  $\text{A}\beta(1-40)$  amyloid fibril as well as the non-convalent bonding models for  $\text{Cu}^{2+}$ -ligand interactions. Although further studies are needed to fully understand  $\text{Cu}^{2+}$  binding structure to  $\text{A}\beta$ , including its relation to the previous EPR studies and a ROS production mechanism, the combination of SSNMR analyses and MD simulations have provided insights into previously unknown detailed structural features of  $\text{Cu}^{2+}$ -bound  $\text{A}\beta(1-40)$  in amyloid fibrils.

The new SSNMR approach presented here may be also applicable to examine binding of small paramagnetic ligands, such as drugs, to amyloid proteins. It has been proposed that metal ions such as  $\text{Cu}^{2+}$  and  $\text{Zn}^{2+}$  may trigger the formation of  $\text{A}\beta$  oligomer or fibril, modulating misfolding kinetics and aggregation states of  $\text{A}\beta$ .<sup>25,30,85</sup> In this initial work, we focused on establishing SSNMR structural analysis of  $\text{A}\beta(1-40)$  fibril upon  $\text{Cu}^{2+}$  binding after fibril formation. A similar approach is likely useful for SSNMR characterization of the structures of  $\text{A}\beta$  oligomer and  $\text{A}\beta$  fibril that are formed in the presence of  $\text{Cu}^{2+}$  or other metal ions.

## Materials and Methods

### Synthesis and purification of $\text{A}\beta(1-40)$ peptide

$\text{A}\beta(1-40)$  peptide (NH<sub>2</sub>-DAEFRHDSGY-EVHHQKLVFF-AEDVGSNKGA-IIGLMVGGVV-COOH) was synthesized and purified as reported previously. Briefly,  $\text{A}\beta(1-40)$  was synthesized using solid-phase peptide synthesis with standard Fmoc synthesis and cleavage protocols.<sup>40,76</sup> The crude peptide was purified by HPLC using acetonitrile and water gradient with 0.1% trifluoroacetic acid. <sup>13</sup>C- and <sup>15</sup>N-labeling was introduced as described previously by incorporating Fmoc-protected uniformly <sup>13</sup>C- and <sup>15</sup>N labeled amino acids at selected residues. The Fmoc protection of the uniformly <sup>13</sup>C- and <sup>15</sup>N-labeled amino acids (Isotec/Sigma-Aldrich, Miamisburg, OH) was performed at the Research Resource Center (RRC) at University of Illinois at Chicago (UIC) using the protocol of Fields et al.<sup>86</sup> The purity of the peptide samples were determined by MALDI-TOF mass spectra performed at UIC RRC and the purity were approximately 95% after the HPLC purification. The purified samples were stored at -20°C before when it was used. The labeling schemes for the 6 samples used are as follows. 1) His-14, Ile-32, Val-36, Gly-37; 2) His-13, Ala-30, Gly-38, Val-39; 3) Val-12, Phe-20, Ala-21, Ile-31, Gly-33, Met-35(<sup>13</sup>C<sub>6</sub>H<sub>3</sub>); 4) Phe-4, Gly-9, Val-12, Leu-17, Ala-21; 5) Phe-19, Val-24, Gly-25, Ala-30, Leu-34; 6) Val-18, Phe-19, Ala-21, Ile-31, Gly-33.

Uniformly <sup>13</sup>C- and <sup>15</sup>N-labeled  $\text{A}\beta(1-40)$  was expressed as a fusion protein with Glutathione S-Transferase (GST) tag connected by a Factor Xa recognition site (IEGR▼) in *E. Coli*. The GST tag was removed by Factor Xa enzymatic cleavage, and then, the peptide was purified by HPLC as described above. The yield of uniformly <sup>15</sup>N- and/or <sup>13</sup>C-protein  $\text{A}\beta(1-40)$  was ~1.5 mg from 1 L of the cell culture. The details of the protocol will be discussed elsewhere.

### Preparation of $\text{A}\beta(1-40)$ fibrils for $\text{Cu}^{2+}$ -binding assay and SSNMR experiments

For  $\text{Cu}^{2+}$ -binding assay with  $\text{A}\beta(1-40)$  fibrils using UV-Vis spectroscopy, a solution of 5 mM  $\text{A}\beta(1-40)$  was prepared by first dissolving  $\text{A}\beta(1-40)$  peptide in 50 mM NaOH.<sup>45</sup> The peptide mixture was then briefly vortexed, and diluted to a final peptide concentration of 500  $\mu\text{M}$  with deionized water containing 0.02 %  $\text{NaN}_3$ . The pH of the solution was adjusted to 7.4 by using 100 mM HCl. The  $\text{A}\beta(1-40)$  solution was sonicated for 5 minutes in an ice

bath, and this solution was then centrifuged at  $16.1 \times 10^3$  g for 5 minutes to remove any preformed aggregates. The peptide solution was divided into several 1.5-mL microvials for Cu<sup>2+</sup>-binding assay. The concentration of Aβ(1–40) was measured using UV-VIS spectroscopy.<sup>40</sup> The Aβ(1–40) solution was then incubated for 14 days with constant agitation in the sample tube at room temperature. Aβ(1–40) fibril formation was confirmed by thioflavin T (ThT) fluorescence assay.

For SSNMR studies, amyloid fibril samples were prepared as described above, but with selectively isotope labeled or uniformly <sup>13</sup>C- and <sup>15</sup>N-labeled Aβ(1–40) peptides. For the samples used for Fig. 1, 2, after incubation of an Aβ solution for fibril formation, the Aβ(1–40) fibril with Cu<sup>2+</sup> was prepared by adding CuCl<sub>2</sub> solution (pH7.4) to the Aβ solution in the mole ratio of 0.4:1.0 (Cu<sup>2+</sup>:Aβ(1–40)), and incubated at 4°C for 24h with initial vortexing. The control sample without Cu<sup>2+</sup> was prepared in the same manner except for the addition of CuCl<sub>2</sub>. The samples were then centrifuged at  $16.1 \times 10^3$  g for about 1 h (20min at a time), and the supernatant was removed. The gel like pellet at the bottom was then lyophilized. The lyophilized Aβ(1–40) fibril samples with and without Cu<sup>2+</sup> were packed in to 2.5mm MAS rotors with rubber O-rings on the spacer and cap. The lyophilized samples were rehydrated with deionized water (3µl water/mg Aβ(1–40)) in the rotor with 3µL of water added at one time, and centrifuged at  $2.0 \times 10^3$  g for 2 min. The hydrated samples were incubated overnight at 4°C before running the SSNMR experiments.

For the uniformly <sup>13</sup>C- and <sup>15</sup>N-labeled Aβ(1–40) fibril sample used for Fig. 3, after incubation for fibril formation, we centrifuged the sample at  $16.1 \times 10^3$  g for ~1.0 h (20 min at a time), and removed the supernatant. The gel-like pellet at the bottom of the centrifugal vial was transferred into the 1.8mm MAS rotor of 10µL volume by centrifugation. The fibrils were then packed into a 1.8 mm rotor by fitting a 200 µL-pipette tip to the rotor with the fibrils and centrifuging the rotor-pipette tip mounted in a micro centrifuge tube with minimum amount of the supernatant for 2 – 4 min at  $6 \times 10^3$  g. Then, the rotor cap was glued with Krazy Glue (Krazy Glue, Columbus OH) with a small piece of Teflon tape between the cap and the sample to avoid interaction of the glue with the peptide. This cap can be removed easily by immersing it in liquid nitrogen. The Aβ(1–40) fibrils with Cu<sup>2+</sup> was prepared by adding a 26.5 mM CuCl<sub>2</sub> solution in the mole ratio of 0.4:1.0 (Cu<sup>2+</sup> : Aβ(1–40)) into the rotor. Firstly, the hydrated Aβ(1–40) sample in a rotor was lyophilized, and then a CuCl<sub>2</sub> solution was introduced directly into the 1.8mm rotor by centrifugation and the cap was glued as described above. The rotor was then incubated at 4°C for 24h before the SSNMR experiments.

### SSNMR experiments

All the SSNMR experiments were performed with an Infinityplus SSNMR spectrometer from Varian (Fort Collins, CO) with a homebuilt 2.5-mm MAS triple-resonance magic-angle-spinning (MAS) probe or a 1.8-mm MAS triple-resonance MAS probe developed at Dr. Samoson's lab (National Institutes of Chemical Physics and Biophysics, Tallinn, Estonia) at 9.4 T (<sup>1</sup>H frequency of 400.2 MHz) in the double-configuration. For the data in Fig. 1 and 2, the spinning speed was set to  $20,000 \pm 3$  Hz throughout the experiments with cooling air at  $-10^\circ\text{C}$  supplied through a Varian VT stack at a flow rate of ~140 standard-cubic-feet per hour (scfh), which kept the sample temperature at  $\sim 11^\circ\text{C}$ . Approximately, 2.0–3.5 mg of labeled Aβ(1–40) fibril samples were used. In the 1D <sup>13</sup>C CPMAS experiments for Fig. 1 and 2, adiabatic CP transfer was used. During the CP period, the <sup>13</sup>C RF field amplitude was linearly swept from 45 kHz to 65 kHz during a contact time of 1.0 ms while the <sup>1</sup>H RF amplitude was kept constant at 75 kHz. During the detection period, <sup>1</sup>H TPPM decoupling of 90 kHz was employed. The recycle delays for the 1D experiments were 1.8 s. The 1D spectra in Fig.1c and Fig.2c were collected with 1024 scans, and were processed with Gaussian broadening of 20Hz and 150 Hz, respectively. The 1D spectra in

Fig. 2a, b were collected with 4096 scans and processed with Gaussian broadening of 150Hz.

In the 2D experiments for Fig. 1d, a 2D  $^{13}\text{C}/^{13}\text{C}$  correlation pulse sequence with the fpRFDR mixing was used.<sup>76,87</sup> After the adiabatic CP, signals were recorded during the  $t_1$  period, and then a real or imaginary component of the magnetization was stored along the z axis. Then, during a mixing period, a fpRFDR  $^{13}\text{C}-^{13}\text{C}$  dipolar-recoupling sequence with a mixing time of 1.6 ms and a  $^{13}\text{C}$   $\pi$ -pulse width of 15  $\mu\text{s}$  was used.  $^1\text{H}$  TPPM decoupling of 90 kHz was employed during the  $t_1$  and  $t_2$  periods, while cw decoupling of the same amplitude was used during the mixing period. For each  $t_1$  point, 192 scans of signals were accumulated with an acquisition period of 10 ms. A total of 180 complex  $t_1$  points were recorded with a  $t_1$  increment of 33.4  $\mu\text{s}$ . The obtained NMR data were processed by NMRPipe software.<sup>88</sup> Gaussian window functions of 110 Hz and 90 Hz were applied along the  $t_1$  and  $t_2$  time domains. An overall experimental time was 35 hours. The experiments were performed for the 6 A $\beta$  samples listed above in which different residues are uniformly  $^{13}\text{C}$ - and  $^{15}\text{N}$ -labeled.  $^{15}\text{N}$ -labeling was introduced for experiments to be performed in the future.

The spectra in Fig. 3 were acquired at a spinning speed of  $40,000 \pm 10$  Hz with cooling air at  $-20^\circ\text{C}$  supplied through a Varian VT stack at a flow rate of  $\sim 140$  scfh with cooled bearing air ( $1^\circ\text{C}$ ), which kept sample temperature at  $\sim 12^\circ\text{C}$ . The 2D  $^{13}\text{C}/^{13}\text{C}$  correlation spectra were obtained using fpRFDR mixing of 1.6 ms with  $^{13}\text{C}$   $\pi$ - pulse widths of 13  $\mu\text{s}$ . Approximate amount of the A $\beta$  fibril sample (excluding water) was  $\sim 0.6$  mg. The  $\pi/2$ -pulse for proton excitation was 2.5  $\mu\text{s}$ . During the 1 ms CP period, the  $^{13}\text{C}$  rf field was swept from 48 kHz to 76 kHz, while the  $^1\text{H}$  rf field was kept at 102 kHz. The signal was collected during an acquisition period of 10 ms with low-power TPPM (lpTPPM)  $^1\text{H}$  decoupling with the rf field intensity ( $\omega_1/2\pi$ ) at 7 kHz was applied with phase alternation between  $\pm 17^\circ$ . A total of 126 complex  $t_1$  points were recorded with a  $t_1$  increment 48  $\mu\text{s}$ . For each  $t_1$  point, 728 scans of signals were accumulated. For the uniformly  $^{13}\text{C}$ - and  $^{15}\text{N}$ -labeled A $\beta$  fibril sample without Cu $^{2+}$ , total experimental time was 72 hours with recycle delays of 1.4 s. For the sample with 0.4 molar eq. of Cu $^{2+}$ , the experiment was collected using PACC method<sup>45</sup> with a total experimental time of 8 hours and recycle delays of 150 ms. The details of the pulse program and lpTPPM are described elsewhere.<sup>45,89</sup> The obtained NMR data were processed by NMR pipe software. Lorentz to Gaussian window functions with inverse exponential width of 30Hz and Gaussian broadening of 80Hz were applied for both  $t_1$  and  $t_2$  time domains.

### Molecular dynamics (MD) simulations protocol

In order to identify possible Cu $^{2+}$  binding structures in A $\beta$ (1–40) fibrils and verify their structural stabilities, we have performed two sets of molecular dynamics (MD) simulations. In the first set of the MD simulations related to the structure shown in Figs. 4–5, we used the structural refinement within AMBER 890. MD simulations were performed using a modified AMBER ff99sb force-field<sup>91</sup> with generalized Born (GB) implicit solvation<sup>92</sup> on an Argo Beowulf PC cluster at the Academic Computing and Communications Center at UIC (<http://www.uic.edu/depts/accc/hardware/argo/index.html>). The AMBER refinement scheme used herein is a slightly modified version which has been used for a number of NMR structure refinements.<sup>93</sup> Force-fields for Cu $^{2+}$  were adopted from those for Zn $^{2+}$  denoted as *tetrahedral divalent cation* model and used with a minor modification with the differences in the atomic mass (65.360) and vdW radius for copper ( $r^* = 3.100$  Å).<sup>78</sup> Although it is possible that Cu $^{2+}$  bound to A $\beta$  takes other coordinates such as a distorted planer geometries suggested by EPR studies,<sup>19,21</sup> we assumed this tetrahedral geometry in order to identify possible metal binding structures for one of the most common Cu $^{2+}$  geometries. It is interesting to note, however, that for the *undistorted* tetrahedral model of

$\text{Cu}^{2+}$  used herein, the ligands can readily sample and coordinate in a distorted fashion (Table S2). Thus, there is indeed some flexibility with regard to how the ligands can arrange around the Cu ions in the CaDa model. In a recent study to simulate  $\text{Cu}^{2+}$ -binding to  $\text{A}\beta(1-40)$ , Baik *et al* showed that the optimization of  $\text{Cu}^{2+}$  coordination to His by ab-initio calculations resulted in the distorted tetrahedral symmetry.<sup>18</sup> A comparison of the coordination geometries for the MD structures for Cu, Zn SOD obtained with different types of force fields with X-ray structure showed that the structural parameters obtained by the tetrahedral model show reasonable agreement with those for the X-ray structure (see Table S2 in SI). A recent X-ray study suggested that Cu, Zn-superoxide dismutase (SOD), a type II  $\text{Cu}^{2+}$  protein, which has a distorted square-planar  $\text{Cu}^{2+}$  coordination geometry, show very limited changes in the coordination structure by replacement of  $\text{Cu}^{2+}$  with  $\text{Zn}^{2+}$  (i.e. Zn, Zn SOD).<sup>94</sup> This is consistent with our MD simulation results with the Cu-CaDa tetrahedral model in SI. The initial structure of the  $\text{A}\beta(1-40)$  fibril was adopted from Tycko's model<sup>77</sup> and the missing 8 N-terminal amino acids were built back into the molecule using Molmol.<sup>95</sup> Based on our NMR data, two sets of initial  $\text{Cu}^{2+}$  locations (i.e at His-13 or His-14) were assumed;  $\text{Cu}^{2+}$  was non-covalently attached to  $\text{N}_e$  of His-13 for Fig. 4 (or His-14 for Fig. 5) by replacement of the  $\text{H}_e$  and held in position by the incorporation of an NOE between the  $\text{Cu}^{2+}$  atom and  $\text{N}_e$  of His with a square well potential varying from 1.6–3.0 Å and a force constant of 10 kcal/mol. Protons at the  $\text{N}_g$  positions of  $\text{Cu}^{2+}$ -bound His-13/14 were removed, while those for other histidines were retained. All hydrogen atom bond lengths were constrained using the SHAKE algorithm.<sup>96</sup> A cutoff of 12 Å was used for nonbonded interactions. Steepest descent minimization was performed for 2000 steps prior to and after MD refinement. The final MD structures were obtained after three thermal annealing cycles (0 K → 1000 K → 0 K) for a total of 60 ps run time. During the MD simulations the coordinates of residues 16–39 were fixed using a harmonic potential of 20 kcal/mol. Based on our NMR results, the structure of these regions is likely to be unaffected by  $\text{Cu}^{2+}$ -binding. As shown in Fig. 4a and Fig. 5a, respectively, many  $\text{Cu}^{2+}$  ions remained attached to His-13 and His-14 via ionic interactions even after three thermal cycles, while some ions dissociated from the positions. Although previous EPR studies predicted only two major  $\text{Cu}^{2+}$  binding structures, coexistence of a variety of binding modes was observed in our MD simulations. The simulations provided insights into the possible metal binding structures.

The second set of MD simulations in Fig. 6 was used to rigorously compare the stability of the  $\text{Cu}^{2+}$  binding structures for three possible binding modes. For the conformation energy calculations in Table 1, MD simulations of solvated  $8\text{Cu}^{2+}\text{-A}\beta(1-40)$  oligomers were also performed in NPT ensemble using the NAMD program<sup>97</sup> and the CHARMM package<sup>98</sup> with the all-atom CHARMM27 force field. The oligomers were explicitly solvated with TIP3P water molecules. Constant temperature (300 K) and constant pressure (1 atm) were controlled by Langevin thermostat with a damping coefficient of 10  $\text{ps}^{-1}$ , using the NAMD program. For simulations using the NAMD program<sup>97</sup>, the Langevin piston method<sup>97,99,100</sup> with a decay period of 100 fs, and a damping time of 50 fs was used to maintain a constant pressure of 1 atm. The short-range van der Waals (VDW) interactions were calculated using the switching function, with a twin range cutoff of 10.0 and 12.0 Å. Long-range electrostatic interactions were calculated using the particle mesh Ewald method with a cut-off of 12.0 Å for all simulations. The equations of motion were integrated using the leapfrog integrator with a step of 1 fs. All initial  $8\text{Cu}^{2+}\text{-A}\beta(1-40)$  oligomer was minimized and then solvated in a TIP3P water box with a minimum distance of 15 Å from any edge of the box to any A $\beta$  atom. Any water molecule within 2.5 Å of the A $\beta$  was removed. Even with  $\text{Cu}^{2+}$  binding, the overall charge for  $\text{Cu}^{2+}\text{-A}\beta(1-40)$  is still -1. Therefore, counter ions ( $\text{Na}^+$ ) were added into solution at random locations to neutralize the charge of  $\text{Cu}^{2+}\text{-A}\beta(1-40)$ . The solvated systems were minimized for 2000 conjugated gradient steps, with the distance between the  $\beta$ -sheets fixed in the range 2.2 – 2.5 Å. The VDW parameters of  $\text{Cu}^{2+}$  ion and all  $\text{Cu}^{2+}$ -ligands distances were constrained to the

estimated distances,<sup>101</sup> both along the minimization process and during all dynamics simulation timescales. Counter ions, peptides and water molecules were all allowed to move. The hydrogen atoms were constrained to the equilibrium bond using the SHAKE algorithm.<sup>96</sup> The minimized solvated systems were quickly heated to 250 K, where all atoms were allowed to move. Then, the systems were heated from 250 K to 300 K for 300 ps and equilibrated at 300 K for 300 ps. Simulations ran for 20 ns and structures were saved every 10 ps for analysis.

Copper-binding octamer was constructed from Tycko's amyloid fibril model.<sup>77</sup> We used one monomer from the fibril conformation of A $\beta$ (9–40). Residues G9–K16 were removed from each monomer and the N-terminal fragment peptide (D1–K16) was linked binding to Cu<sup>2+</sup>. The initial conformation of Cu<sup>2+</sup>-A $\beta$ (1–16) was combined with the A $\beta$ (17–40) as follows. The Zn<sup>2+</sup> ions in the solution NMR structure of Zn<sup>2+</sup>-A $\beta$ (1–16) complex from Zirah *et al.*<sup>102</sup> were replaced with the Cu<sup>2+</sup> ion. Then, all Cu<sup>2+</sup>-ligands distances were constrained to the estimated distances with the residues that coordinate with the ions. Based on previous EPR and NMR studies,<sup>19–21,27</sup> two conformers were tested where Cu<sup>2+</sup> binds to residues in the N-terminal: in the first model, Cu<sup>2+</sup> binds to H6, H13 and H14 (Conformer 1; Figure 6a) and in the second model, Cu<sup>2+</sup> interacts with D1, H6 and H14 (Conformer 2; Figure 6b). To test interactions of the copper ions with the C-termini of A $\beta$  suggested in the SSNMR data and CaDa MD simulation, we constructed a model with 4 Cu<sup>2+</sup> ions coordinating to D1, H14 and V40; and 4 Cu<sup>2+</sup> ions to D1, H6 and H14 (Conformer 3; Figure 6c) and another model with 4 Cu<sup>2+</sup> ions coordinating to D1, H14 and V40; and 4 Cu<sup>2+</sup> ions to D1, H6 and H13 (Conformer 4; Figure 6d).

**Analysis details for MD simulations**—To obtain the relative structural stability of the 8Cu<sup>2+</sup>-A $\beta$ (1–40) oligomers listed in Table 1, the A $\beta$  trajectories of the last 5 ns were first extracted from the explicit MD simulation excluding water molecules. The solvation energies of all systems were calculated using the Generalized Born Method with Molecular Volume (GBMV).<sup>103,104</sup> In the GBMV calculations, the dielectric constant of water was set to 80.0 and no distance cutoff was used. The hydrophobic solvent-accessible surface area (SASA) term factor was set to 0.00592 kcal/mol·Å<sup>2</sup>. Each conformer is minimized for 1000 cycles and the conformation energy is evaluated by grid-based GBMV. The minimization does not change the conformations of each conformer, but only relaxed the local geometries due to thermal fluctuation which occurred during the MD simulations.

The relative conformational stabilities of the oligomers were measured by root mean-squared deviation (RMSD) of the C-terminal region (residues Leu17–Val40), the N-terminal region (residues Ala2–Gln15) and for the U-turn region (residues Glu22–Gly29) with respect to the initial minimized structure throughout the simulations. We also examined the stability of the oligomers by following changes in the number of hydrogen bonds between the  $\beta$  strands with the hydrogen bond cutoff set to 2.5 Å (Fig. S7a) and by monitoring the change in the inter-sheet distance (C $\alpha$  backbone-backbone distance) in the core domains of all oligomers (Ala-21–Ile-31 distance; Fig. S7b). The latter distance is the averaged distance between each two  $\beta$ -sheet regions near to the salt bridge in each monomer for each conformer.

## Supplementary Material

Refer to Web version on PubMed Central for supplementary material.

## Acknowledgments

This study was supported primarily by NIH RO1 program (AG028490), and the Alzheimer's Association grant (IIRG 08-91256). The SSNMR methodology development in this work was also supported by the NSF (CHE 449952, CHE 957793), and the Dreyfus Foundation Teacher-Scholar Award program. This project has been funded in part with Federal funds from the NCI, NIH under contract number HHSN261200800001E. Simulations were also performed on the Biowulf cluster at the NIH (<http://biowulf.nih.gov>). We thank Dr. Robert Tycko at the NIH for providing a pdb file of the structural model for A $\beta$ (1–40) fibril and the A $\beta$  fibrils samples used for Fig. S3 in SI. We are also grateful to Prof. Michael Zagorski at the Case Western Reserve University for kind clarifications on his works.

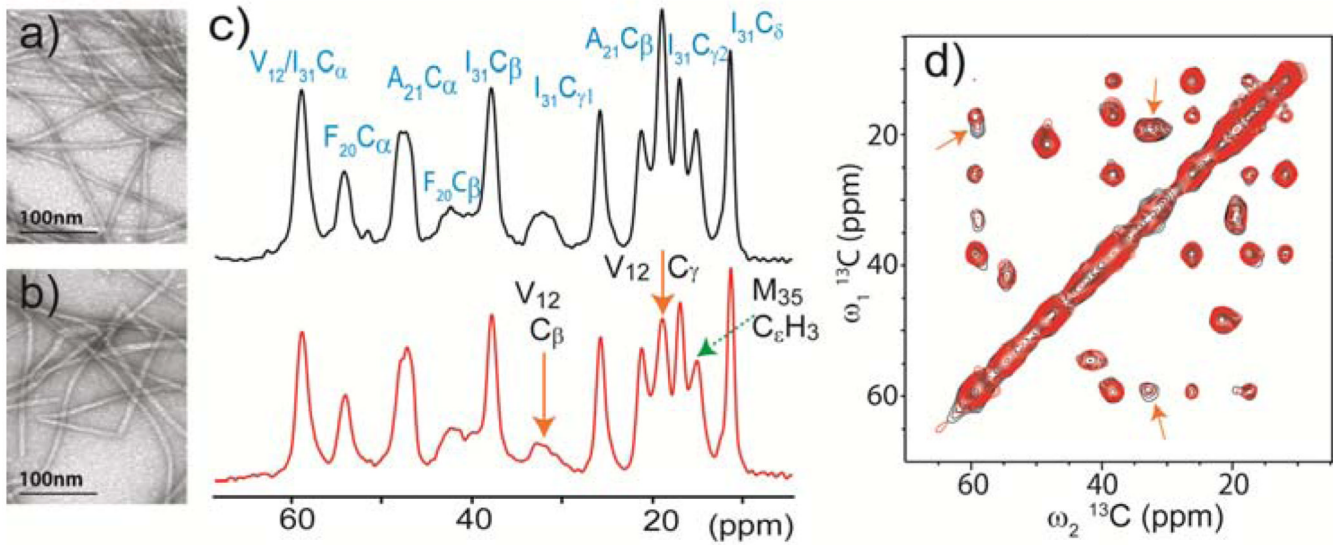
## References

1. Mattson MP. *Nature*. 2004; 430:631–639. [PubMed: 15295589]
2. Selkoe DJ. *Nat. Cell. Biol.* 2004; 6:1054–1061. [PubMed: 15516999]
3. Lovell MA, Robertson JD, Teesdale WJ, Campbell JL, Markesberry WR. *Journal of the Neurological Sciences*. 1998; 158:47–52. [PubMed: 9667777]
4. Leskovjan AC, Lanzirotti A, Miller LM. *Neuroimage*. 2009; 47:1215–1220. [PubMed: 19481608]
5. Miller LM, Wang Q, Telivala TP, Smith RJ, Lanzirotti A, Miklossy J. *J. Struct. Biol.* 2006; 155:30–37. [PubMed: 16325427]
6. Huang XD, Atwood CS, Hartshorn MA, Multhaup G, Goldstein LE, Scarpa RC, Cuajungco MP, Gray DN, Lim J, Moir RD, Tanzi RE, Bush AI. *Biochemistry*. 1999; 38:7609–7616. [PubMed: 10386999]
7. Ali FE, Separovic F, Barrow CJ, Cherny RA, Fraser F, Bush AI, Masters CL, Barnham KJ. *J. Pept. Sci.* 2005; 11:353–360. [PubMed: 15635660]
8. Faller P. *ChemBioChem*. 2009; 10:2837–2845. [PubMed: 19877000]
9. Opazo C, Huang XD, Cherny RA, Moir RD, Roher AE, White AR, Cappai R, Masters CL, Tanzi RE, Inestrosa NC, Bush AI. *J. Biol. Chem.* 2002; 277:40302–40308. [PubMed: 12192006]
10. Scott LE, Orvig C. *Chem. Rev.* 2009; 109:4885–4910. [PubMed: 19637926]
11. Atwood CS, Scarpa RC, Huang XD, Moir RD, Jones WD, Fairlie DP, Tanzi RE, Bush AI. *J. Neurochem.* 2000; 75:1219–1233. [PubMed: 10936205]
12. Atwood CS, Moir RD, Huang XD, Scarpa RC, Bacarra NME, Romano DM, Hartshorn MK, Tanzi RE, Bush AI. *J. Biol. Chem.* 1998; 273:12817–12826. [PubMed: 9582309]
13. Bush AI, Tanzi RE. *Proc. Natl. Acad. Sci. U. S. A.* 2002; 99:7317–7319. [PubMed: 12032279]
14. Bush AI. *J. Alz. Dis.* 2008; 15:223–240.
15. Barnham KJ, Kenche VB, Ciccotosto GD, Smith DP, Tew DJ, Liu X, Perez K, Cranston GA, Johanssen TJ, Volitakis I, Bush AI, Masters CL, White AR, Smith JP, Cherny RA, Cappai R. *Proc. Natl. Acad. Sci. U. S. A.* 2008; 105:6813–6818. [PubMed: 18463291]
16. Choi J-S, Braymer JJ, Nanga RPR, Ramamoorthy A, Lim MH. *Proc. Natl. Acad. Sci. U. S. A.* 2010; 107:21990–21995. [PubMed: 21131570]
17. Jun S, Gillespie JR, Shin B-k, Saxena S. *Biochemistry*. 2009; 48:10724–10732. [PubMed: 19824649]
18. Mantri Y, Fioroni M, Baik MH. *J. Biol. Inorg. Chem.* 2008; 13:1197–1204. [PubMed: 18607649]
19. Drew SC, Noble CJ, Masters CL, Hanson GR, Barnham KJ. *J. Am. Chem. Soc.* 2009; 131:1195–1207. [PubMed: 19119811]
20. Drew SC, Masters CL, Barnham KJ. *J. Am. Chem. Soc.* 2009; 131:8760–8761. [PubMed: 19496610]
21. Sarell CJ, Syme CD, Rigby SEJ, Viles JH. *Biochemistry*. 2009; 48:4388–4402. [PubMed: 19338344]
22. Minicozzi V, Stellato F, Comai M, Serra MD, Potrich C, Meyer-Klaucke W, Morante S. *J. Biol. Chem.* 2008; 283:10784–10792. [PubMed: 18234670]
23. Ali FE, Separovic F, Barrow CJ, Yao SG, Barnham KJ. *Int. J. Pept. Res. Ther.* 2006; 12:153–164.
24. Gaggelli E, Grzonka Z, Kozlowski H, Migliorini C, Molteni E, Valensin D, Valensin G. *Chem. Commun.* 2008;341–343.

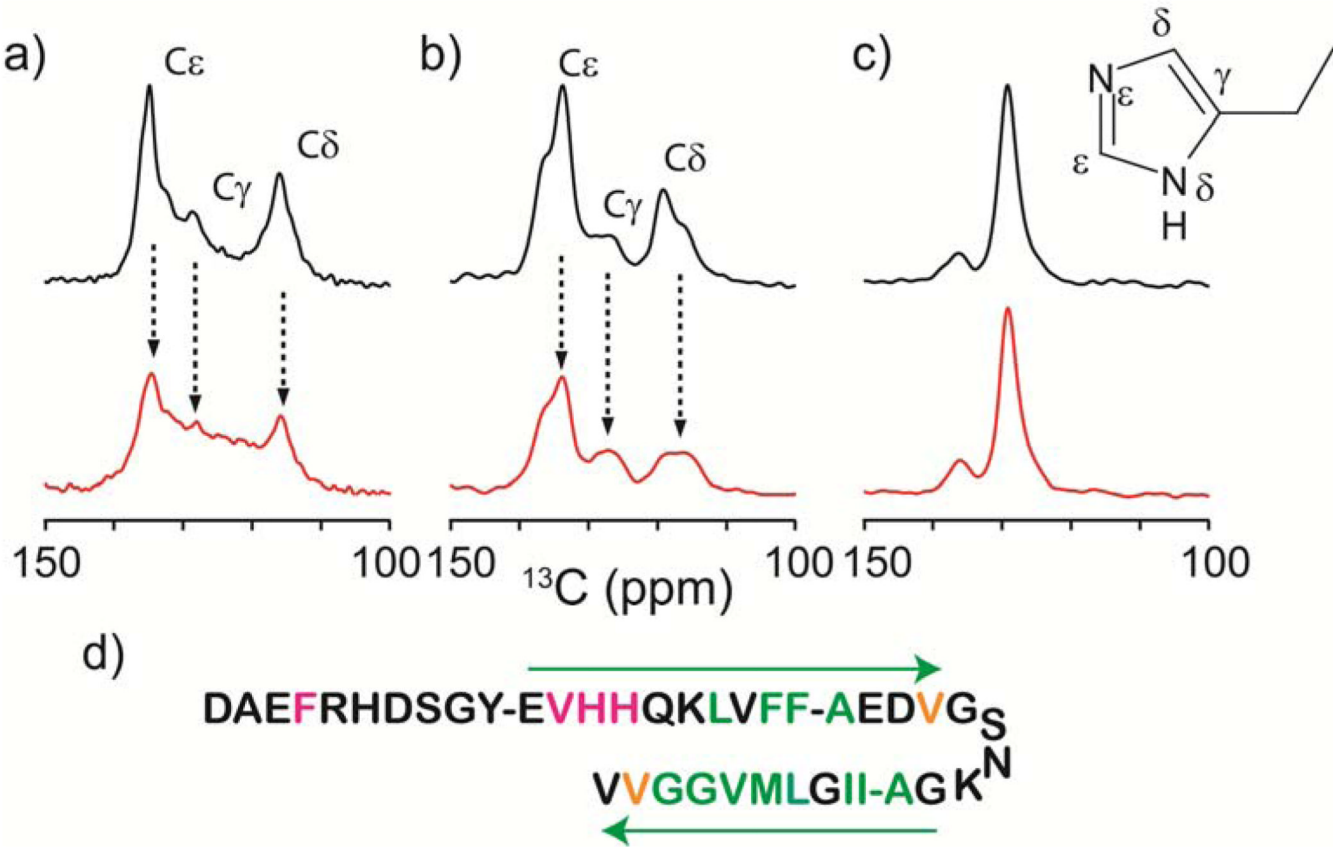
25. Lim KH, Kim YK, Chang YT. *Biochemistry*. 2007; 46:13523–13532. [PubMed: 17973493]
26. Miura T, Suzuki K, Kohata N, Takeuchi H. *Biochemistry*. 2000; 39:7024–7031. [PubMed: 10841784]
27. Hou LM, Zagorski MG. *J. Am. Chem. Soc.* 2006; 128:9260–9261. [PubMed: 16848423]
28. Karr JW, Kaupp LJ, Szalai VA. *J. Am. Chem. Soc.* 2004; 126:13534–13538. [PubMed: 15479110]
29. Karr JW, Szalai VA. *J. Am. Chem. Soc.* 2007; 129 3796–+
30. Liu ST, Howlett G, Barrow CJ. *Biochemistry*. 1999; 38:9373–9378. [PubMed: 10413512]
31. Antzutkin ON. *Magn. Reson. Chem.* 2004; 42:231–246. [PubMed: 14745804]
32. Hindo SS, Mancino AM, Braymer JJ, Liu YH, Vivekanandan S, Ramamoorthy A, Lim MH. *J. Am. Chem. Soc.* 2009; 131 16663–+
33. Olofsson A, Lindhagen-Persson M, Vestling M, Sauer-Eriksson AE, Ohman A. *Febs Journal*. 2009; 276:4051–4060. [PubMed: 19549187]
34. Zoroddu MA, Medici S, Peana M. *J. Inorg. Biochem.* 2009; 103:1214–1220. [PubMed: 19647321]
35. Karr JW, Szalai VA. *Biochemistry*. 2008; 47:5006–5016. [PubMed: 18393444]
36. Petkova A, Ishii Y, Balbach JJ, Antzutkin ON, Leapman RD, Delaglio F, Tycko R. *Proc. Natl. Acad. Sci. U. S. A.* 2002; 99:16742–16747. [PubMed: 12481027]
37. Heise H, Hoyer W, Becker S, Andronesi OC, Riedel D, Baldus M. *Proc. Natl. Acad. Sci. U. S. A.* 2005; 102:15871–15876. [PubMed: 16247008]
38. Chimon S, Ishii Y. *J. Am. Chem. Soc.* 2005; 127:13472–13473. [PubMed: 16190691]
39. Sciarretta KL, Gordon DJ, Petkova AT, Tycko R, Meredith SC. *Biochemistry*. 2005; 44:6003–6014. [PubMed: 15835889]
40. Chimon S, Shaibat MA, Jones CR, Calero DC, Aizezi B, Ishii Y. *Nat. Struct. Mol. Biol.* 2007; 14:1157–1164. [PubMed: 18059284]
41. Wasmer C, Soragni A, Sabate R, Lange A, Riek R, Meier BH. *Angew. Chem. Int. Edit.* 2008; 47:5839–5841.
42. Helmus JJ, Surewicz K, Nadaud PS, Surewicz WK, Jaroniec CP. *Proc. Natl. Acad. Sci. U. S. A.* 2008; 105:6284–6289. [PubMed: 18436646]
43. Curtis-Fisk J, Spencer RM, Weliky DP. *J. Am. Chem. Soc.* 2008; 130 12568–+
44. Jaroniec CP, MacPhee CE, Astrof NS, Dobson CM, Griffin RG. *Proc. Natl. Acad. Sci. U. S. A.* 2002; 99:16748–16753. [PubMed: 12481032]
45. Wickramasinghe NP, Parthasarathy S, Jones CR, Bhardwaj C, Long F, Kotecha M, Mehboob S, Fung LWM, Past J, Samoson A, Ishii Y. *Nat. Methods*. 2009; 6:215–218. [PubMed: 19198596]
46. Masuda Y, Uemura S, Ohashi R, Nakanishi A, Takegoshi K, Shimizu T, Shirasawa T, Irie K. *Chembiochem*. 2009; 10:287–295. [PubMed: 19115328]
47. Pintacuda G, Giraud N, Picrattelli R, Bockmann A, Bertini I, Emsley L. *Angew. Chem. Int. Edit.* 2007; 46:1079–1082.
48. Balayssac S, Bertini I, Lelli M, Luchinat C, Maletta M. *J. Am. Chem. Soc.* 2007; 129:2218–2219. [PubMed: 17266313]
49. Balayssac S, Bertini I, Bhaumik A, Lelli M, Luchinat C. *Proc. Natl. Acad. Sci. U. S. A.* 2008; 105:17284–17289. [PubMed: 18988744]
50. Pooransingh-Margolis N, Renirie R, Hasan Z, Wever R, Vega AJ, Polenova T. *J. Am. Chem. Soc.* 2006; 128:5190–5208. [PubMed: 16608356]
51. Castellani F, van Rossum B, Diehl A, Schubert M, Rehbein K, Oschkinat H. *Nature*. 2002; 420:98–102. [PubMed: 12422222]
52. Morcombe CR, Gaponenko V, Byrd RA, Zilm KW. *J. Am. Chem. Soc.* 2005; 127:397–404. [PubMed: 15631490]
53. Lorieau JL, Day LA, McDermott AE. *Proc. Natl. Acad. Sci. U. S. A.* 2008; 105:10366–10371. [PubMed: 18653759]
54. Qiang W, Bodner ML, Weliky DP. *J. Am. Chem. Soc.* 2008; 130:5459–5471. [PubMed: 18370385]
55. Lange A, Giller K, Hornig S, Martin-Eauclaire MF, Pongs O, Becker S, Baldus M. *Nature*. 2006; 440:959–962. [PubMed: 16612389]

56. Cady SD, Schmidt-Rohr K, Wang J, Soto CS, DeGrado WF, Hong M. *Nature*. 2010; 463:689–U127.
57. Hu FH, Luo WB, Hong M. *Science*. 2010; 330:505–508. [PubMed: 20966251]
58. Sharma M, Yi MG, Dong H, Qin HJ, Peterson E, Busath DD, Zhou HX, Cross TA. *Science*. 2010; 330:509–512. [PubMed: 20966252]
59. Griffin RG. *Nat. Struct. Biol.* 1998; 5:508–512. [PubMed: 9665180]
60. Opella SJ. *Nat. Struct. Biol.* 1997; 4:845–848. [PubMed: 9377156]
61. McDermott AE. *Curr. Opin. Struct. Biol.* 2004; 14:554–561. [PubMed: 15465315]
62. Baldus M. *Curr. Opin. Struct. Biol.* 2006; 16:618–623. [PubMed: 16942870]
63. Gehman JD, O'Brien CC, Shabanpoor F, Wade JD, Separovic F. *Eur. Biophys. J. Biophys. Lett.* 2008; 37:333–344.
64. Bertini I, Emsley L, Lelli M, Luchinat C, Mao JF, Pintacuda G. *J. Am. Chem. Soc.* 2010; 132:5558–.
65. Jovanovic T, McDermott AE. *J. Am. Chem. Soc.* 2005; 127:13816–13821. [PubMed: 16201802]
66. Wickramasinghe NP, Shaibat MA, Ishii Y. *J. Phys. Chem. B*. 2007; 111:9693–9696. [PubMed: 17661508]
67. Nadaud PS, Helmus JJ, Kall SL, Jaroniec CP. *J. Am. Chem. Soc.* 2009; 131:8108–8120. [PubMed: 19445506]
68. Miller Y, Ma BY, Nussinov R. *Proc. Natl. Acad. Sci. U. S. A.* 2010; 107:9490–9495. [PubMed: 20448202]
69. Smith DP, Smith DG, Curtain CC, Boas JF, Pilbrow JR, Ciccotosto GD, Lau TL, Tew DJ, Perez K, Wade JD, Bush AI, Drew SC, Separovic F, Masters CL, Cappai R, Barnham KJ. *J. Biol. Chem.* 2006; 281:15145–15154. [PubMed: 16595673]
70. Petkova AT, Leapman RD, Guo ZH, Yau WM, Mattson MP, Tycko R. *Science*. 2005; 307:262–265. [PubMed: 15653506]
71. Matsuba Y, Takahashi Y. *Analytical Biochemistry*. 1970; 36:182–&.
72. Varadarajan S, Kanski J, Aksanova M, Lauderback C, Butterfield DA. *J. Am. Chem. Soc.* 2001; 123:5625–5631. [PubMed: 11403592]
73. Schoneich C, Pogocki D, Hug GL, Bobrowski K. *J. Am. Chem. Soc.* 2003; 125:13700–13713. [PubMed: 14599209]
74. Barnham KJ, Ciccotosto GD, Tickler AK, Ali FE, Smith DG, Williamson NA, Lam YH, Carrington D, Tew D, Kocak G, Volitakis I, Separovic F, Barrow CJ, Wade JD, Masters CL, Cherny RA, Curtain CC, Bush AI, Cappai R. *J. Biol. Chem.* 2003; 278:42959–42965. [PubMed: 12925530]
75. Tickler AK, Smith DG, Ciccotosto GD, Tew DJ, Curtain CC, Carrington D, Masters CL, Bush AI, Cherny RA, Cappai R, Wade JD, Barnham KJ. *J. Biol. Chem.* 2005; 280:13355–13363. [PubMed: 15668252]
76. Petkova A, Ishii Y, Balbach JJ, Antzutkin ON, Leapman RD, Delaglio F, Tycko R. *Proc. Natl. Acad. Sci. U.S.A.* 2002; 99:16742–16747. [PubMed: 12481027]
77. Petkova AT, Yau WM, Tycko R. *Biochemistry*. 2006; 45:498–512. [PubMed: 16401079]
78. Pang YP. *J. Mol. Modeling*. 1999; 5:196–202.
79. Branco RJF, Fernandes PA, Ramos MJ. *J. Phys. Chem. B*. 2006; 110:16754–16762. [PubMed: 16913815]
80. Peters MB, Yang Y, Wang B, Fusti-Molnar L, Weaver MN, Merz KM. *J. Chem. Theory Comput.* 2010; 6:2935–2947. [PubMed: 20856692]
81. Ishii Y, Chimon S, Wickramasinghe NP. *J. Am. Chem. Soc.* 2003; 125:3438–3439. [PubMed: 12643699]
82. Wickramasinghe NP, Shaibat M, Ishii Y. *J. Am. Chem. Soc.* 2005; 127:5796–5797. [PubMed: 15839671]
83. Shaibat MA, Casabianca LB, Wickramasinghe NP, Guggenheim S, de Dios AC, Ishii Y. *J. Am. Chem. Soc.* 2007; 129:10968–.

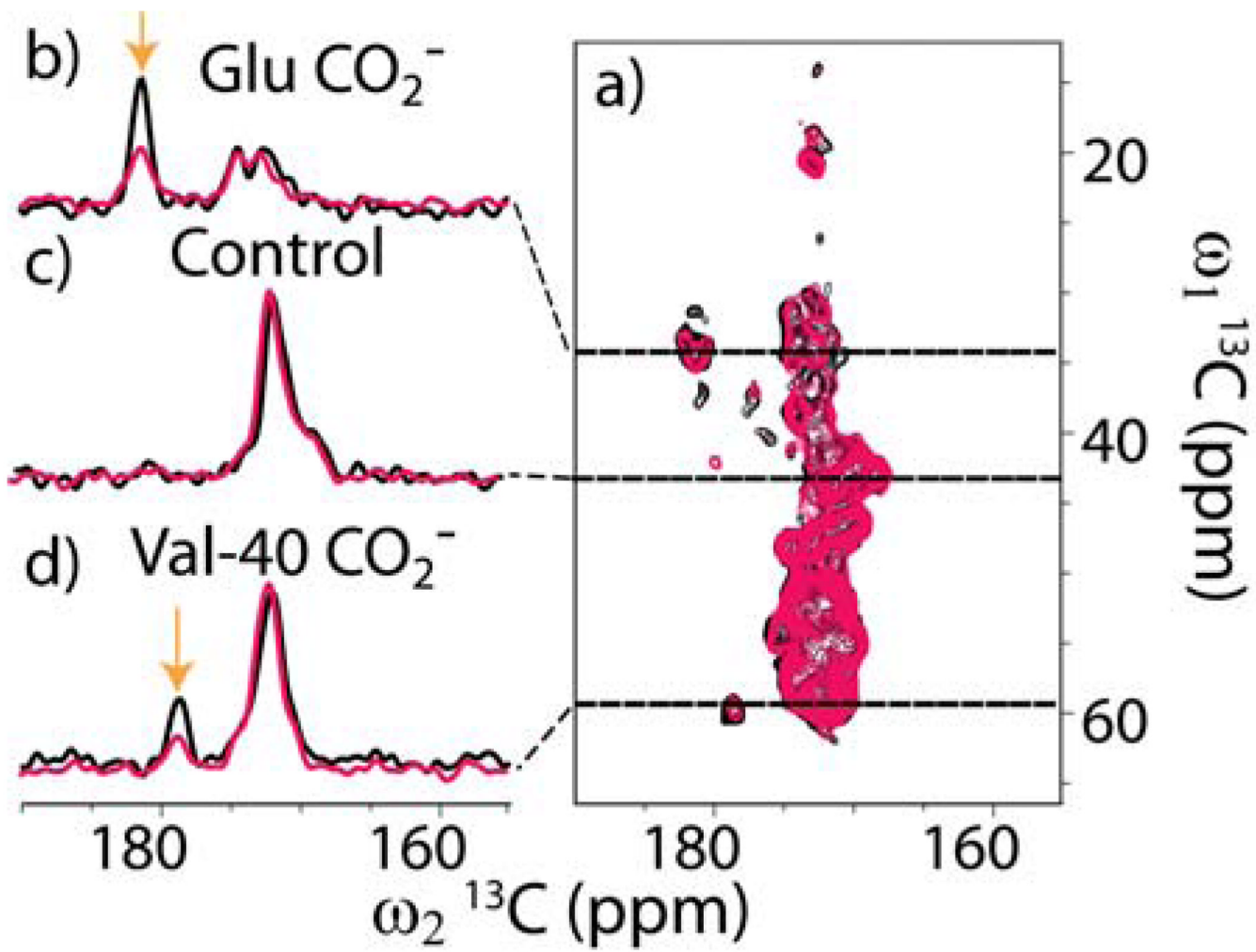
84. Kervern G, Pintacuda G, Zhang Y, Oldfield E, Roukoss C, Kuntz E, Herdtweck E, Bassett JM, Cadars S, Lesage A, Coperet C, Emsley L. *J. Am. Chem. Soc.* 2006; 128:13545–13552. [PubMed: 17031968]
85. Miller Y, Ma B, Nussinov R. *Chem. Rev.* 2010; 110:4820–4838. [PubMed: 20402519]
86. Fields CA, Fields GB, Noble RL, Cross TA. *Int. J. Peptide Protein Res.* 1989; 33:298–303. [PubMed: 2473960]
87. Ishii Y. *J. Chem. Phys.* 2001; 114:8473–8483.
88. Delaglio F, Grzesiek S, Vuister GW, Zhu G, Pfeifer J, Bax A. *J. Biomol. NMR.* 1995; 6:277–293. [PubMed: 8520220]
89. Kotecha M, Wickramasinghe NP, Ishii Y. *Magn. Reson. Chem.* 2007; 45:S221–S230.
90. Case, DAD.; Cheatham, ITE.; Simmerling, CL.; Wang, J.; Duke, RE.; Luo, R.; Merz, KM.; Wang, B.; Pearlman, DA.; Crowley, M.; Brozell, S.; Tsui, V.; Gohlke, H.; Mongan, J.; Hornak, V.; Cui, G.; Beroza, P.; Schafmeister, C.; Caldwell, JW.; Ross, WS.; Kollman, PA. San Francisco: University of California; 2004.
91. Hornak V, Abel R, Okur A, Strockbine B, Roitberg A, Simmerling C. *Proteins-Struct. Funct. Bioinf.* 2006; 65:712–725.
92. Tsui V, Case DA. *J. Am. Chem. Soc.* 2000; 122:2489–2498.
93. Perez-Alvarado GC, Martinez-Yamout M, Allen MM, Grosschedl R, Dyson HJ, Wright PE. *Biochemistry.* 2003; 42:7348–7357. [PubMed: 12809490]
94. Strange RW, Antonyuk SV, Hough MA, Doucette PA, Valentine JS, Hasnain SS. *J. Mol. Biol.* 2006; 356:1152–1162. [PubMed: 16406071]
95. Koradi R, Billeter M, Wuthrich K. *J. Mol. Graph.* 1996; 14 51-&.
96. Ryckaert JP, Ciccotti G, Berendsen HJC. *J. Comput. Phys.* 1977; 23:327–341.
97. Kale L, Skeel R, Bhandarkar M, Brunner R, Gursoy A, Krawetz N, Phillips J, Shinozaki A, Varadarajan K, Schulten K. *J. Comput. Phys.* 1999; 151:283–312.
98. Brooks BR, Bruccoleri RE, Olafson BD, States DJ, Swaminathan S, Karplus M. *J. Comput. Chem.* 1983; 4:187–217.
99. Martyna GJ, Tobias DJ, Klein ML. *J. Chem. Phys.* 1994; 101:4177–4189.
100. Feller SE, Zhang YH, Pastor RW, Brooks BR. *J. Chem. Phys.* 1995; 103:4613–4621.
101. Deng NJ, Yan L, Singh D, Cieplak P. *Biophys. J.* 2006; 90:3865–3879. [PubMed: 16513784]
102. Zirah S, Kozin SA, Mazur AK, Blond A, Cheminant M, Segalas-Milazzo I, Debey P, Rebuffat S. *J. Biol. Chem.* 2006; 281:2151–2161. [PubMed: 16301322]
103. Lee MS, Salsbury FR, Brooks CL. *J. Chem. Phys.* 2002; 116:10606–10614.
104. Lee MS, Feig M, Salsbury FR, Brooks CL. *J. Comput. Chem.* 2003; 24:1348–1356. [PubMed: 12827676]

**Figure 1.**

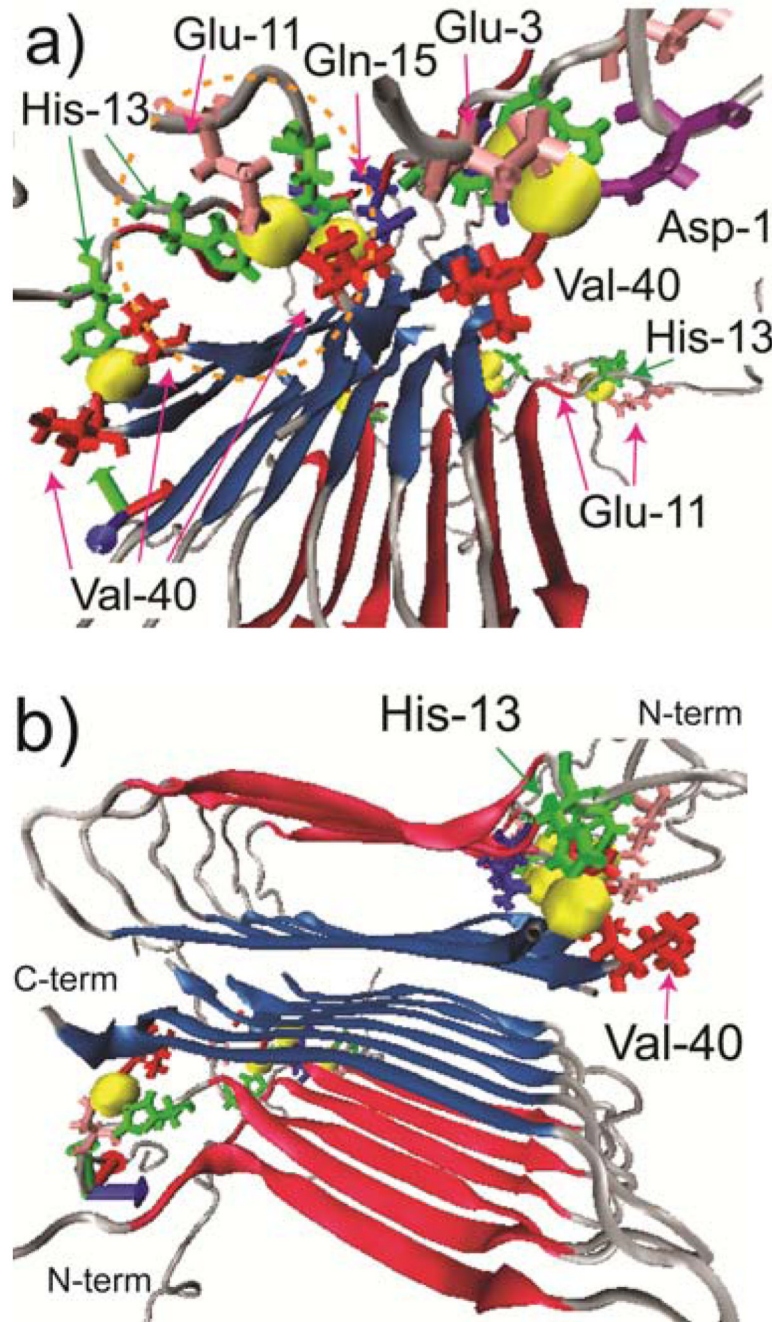
(a, b) Transmission electron microscopy images of A<sub>β</sub>(1-40) fibrils (a) without and (b) with Cu<sup>2+</sup>, which is 0.4 molar equivalence (eq.) to A<sub>β</sub>. Cu<sup>2+</sup> ions were added after the fibril formation was complete throughout this work. (c) Comparison of 1D <sup>13</sup>C CPMAS spectra of A<sub>β</sub>(1-40) fibrils without (black) and with (red) 0.4 molar eq. of Cu<sup>2+</sup>, together with signal assignments. The samples were labeled with uniformly <sup>13</sup>C-, <sup>15</sup>N-labeled amino acids at V12, F20, A21, I31, G33 and with <sup>13</sup>C<sub>e</sub>H<sub>3</sub> selectively labeled at M35. (d) Comparison of the 2D <sup>13</sup>C/<sup>13</sup>C correlation spectra for the same fibrils samples without (black) and with (red) Cu<sup>2+</sup>. The spectra were obtained at magic angle spinning (MAS) at 20 kHz. In (d), a fpRFDR sequence of 1.6 ms87 was used for <sup>13</sup>C-<sup>13</sup>C exchange.

**Figure 2.**

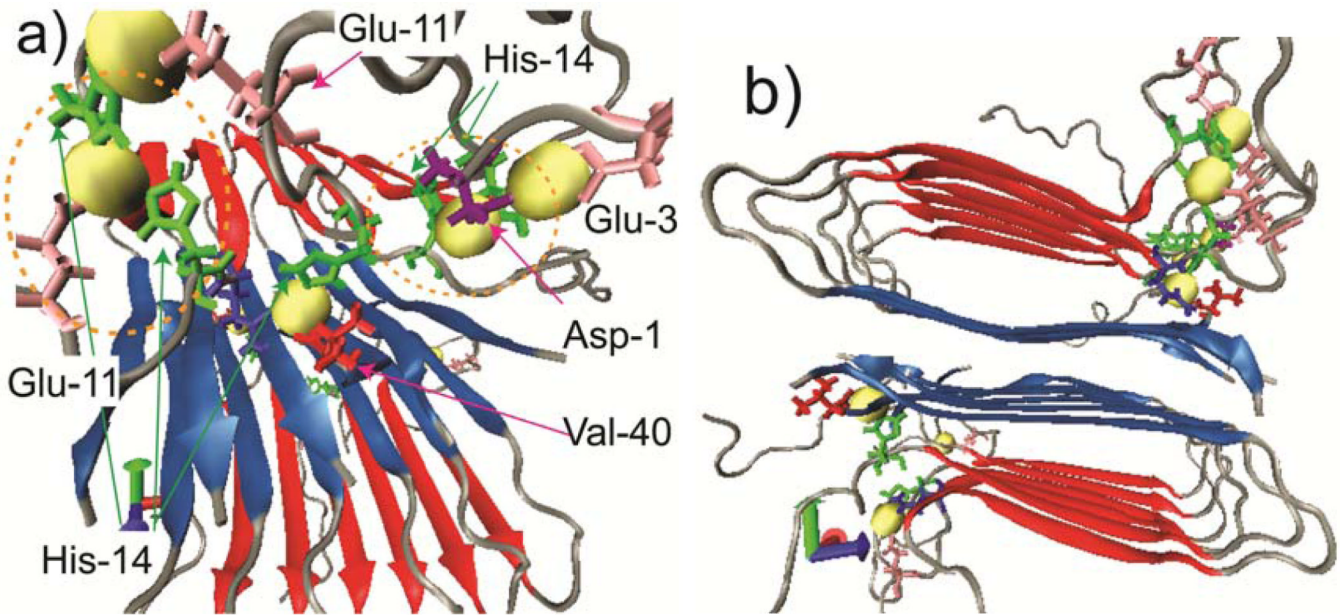
Aromatic regions of <sup>13</sup>C CPMAS spectra for (a) H13, (b) H14, and (c) F20 side chains for A $\beta$ (1–40) fibrils in the hydrated state (black) without and (red) with Cu<sup>2+</sup>. (d) Amino acid sequence of A $\beta$ (1–40) and the extent of signal quenching by Cu<sup>2+</sup> binding (green: 15%; orange: 15%–25%; red: 25%). The quenching is the average of that for all the observed <sup>13</sup>C sites for each residue. The arrow denotes  $\beta$ -sheet regions reported in the previous studies by Tycko et al.<sup>77</sup>

**Figure 3.**

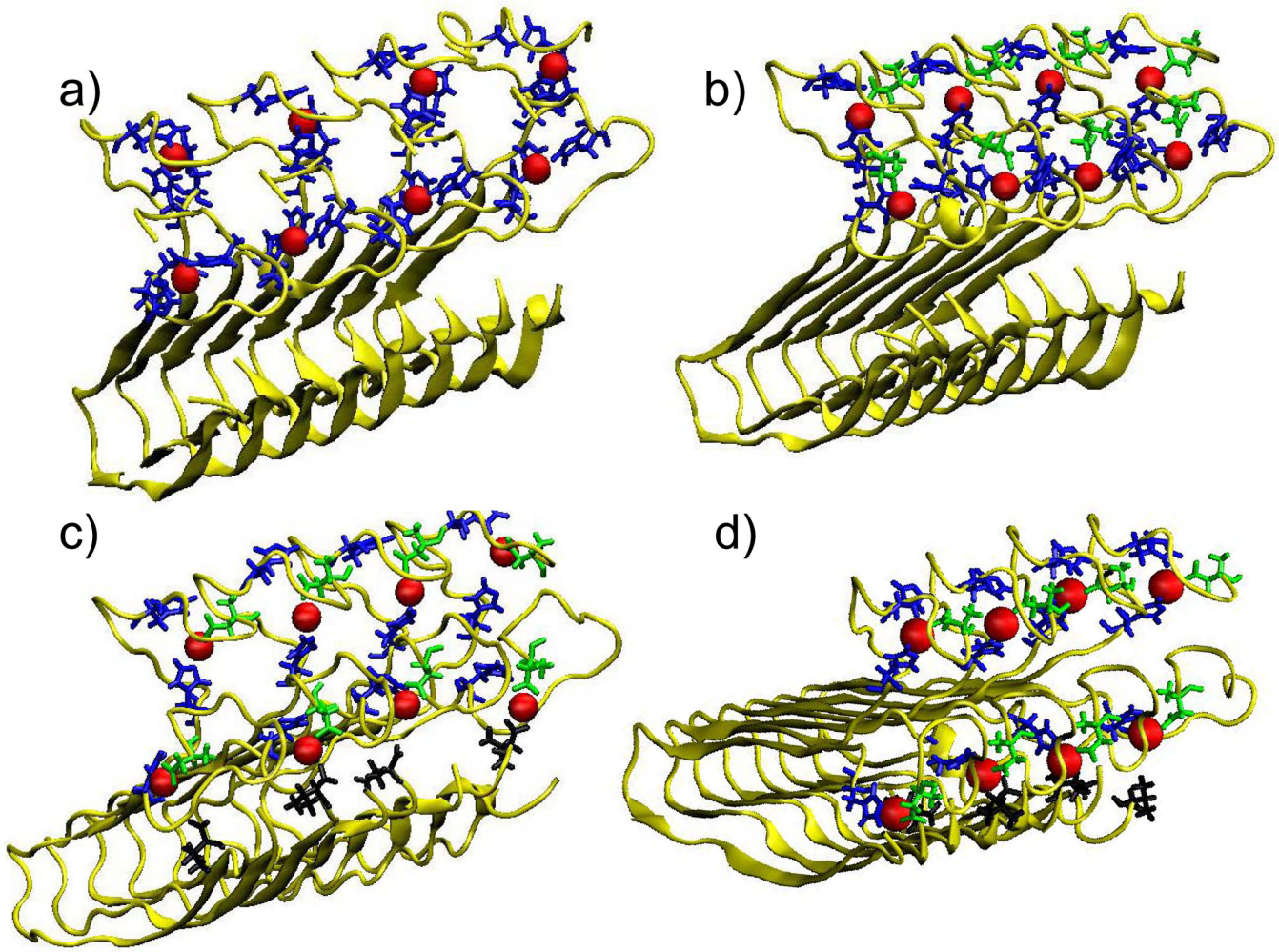
(a) 2D  $^{13}\text{C}/^{13}\text{C}$  SSNMR spectra between aliphatic and  $^{13}\text{CO}$  regions for uniformly  $^{13}\text{C}$ - and  $^{15}\text{N}$ -labeled  $\text{A}\beta(1\text{--}40)$  fibrils (black) without and (red) with  $\text{Cu}^{2+}$ , with 1D slices at  $\omega_1 =$  (b) 34.6, (c) 43.9, (d) 59.8 ppm. The spectra were obtained at MAS of 40 kHz with a fpRFDR mixing of 1.6 ms.87

**Figure 4.**

(a, b) The final MD structure of Cu<sup>2+</sup> bound A<sup>β</sup>(1–40) fibril viewed from (a) one of the N-terminal sides and (b) the fibril axis after three thermal annealing cycles (see SI). In the initial structures, Cu<sup>2+</sup> were bound to N<sub>e</sub> of H13 via non-covalent interactions. Blue and red arrows indicate β-sheet regions in residue 16–24 (red) and residue 30–39 (blue) of A<sup>β</sup>. The MD structure shows that Cu<sup>2+</sup> (yellow) are bound to H13 (green), E3, E11 (pink), D1 (purple), Q15 (blue), and V40 (red) after the thermal cycles. The radius of the Cu<sup>2+</sup> ions' sphere is ~2 Å. The distances between Cu<sup>2+</sup> and some of the ligands are shown in Fig. S4 in SI.

**Figure 5.**

(a, b) The final MD structure of Cu<sup>2+</sup> bound A<sup>β</sup>(1–40) fibril viewed from (a) one of the N-terminal sides and (b) the fibril axis after three thermal annealing cycles. In the initial structures, Cu<sup>2+</sup> were bound to N<sub>e</sub> of His-14 via non-covalent interactions. Blue and red arrows indicate β-sheet regions in residue 16–24 (red) and residue 30–39 (blue) of A<sup>β</sup>. The MD structure show that Cu<sup>2+</sup> (yellow) are bound to His-14 (green), Glu-3, 11 (pink), Asp-1 (purple), Gln-15(blue), and Val-40 (red) after the thermal cycles. The radius of the yellow sphere is ~2 Å from the Cu<sup>2+</sup> ion.

**Figure 6.**

(a) Conformer 1 for which His-6, His-13, His-14 residues are coordinated to copper ions. (b) Conformer 2 for which Asp-1 (green), His-6 (blue), His-14 (blue) residues are coordinated to a copper ion. (c) Conformer 3 for which Asp-1 (green), His-6 (blue), His-14 (blue) residues are coordinated to a copper ion and Asp-1 (green), His-14 (blue), Val-40 (black) are coordinated to another copper ion. (d) Conformer 4 for which Asp-1 (green), His-6 (blue), His-14 (blue) residues are coordinated to a copper ion and Asp-1 (green), His-13 (blue), Val-40 (black) are coordinated to another copper ion. The magnified coordination geometries are shown in Fig. S6 in SI.

**Table 1**

The conformational energy of simulated Cu<sup>2+</sup>-Aβ(1–40) models.

Conformer	Residues coordinated to Cu <sup>2+</sup> <sup>a)</sup>	Conformational energy (kcal/mol) <sup>b)</sup>
1	H6, H13, H14	-11978.1 (205.2)
2	D1, H6, H14	-11857.3 (171.5)
3	D1, H6, H14 and D1, H14, V40	-11873.9 (164.5)
4	D1, H6, H14 and D1, H13, V40	-11901.7 (185.0)

<sup>a)</sup> See Figs. 6 for the modes of the coordination for each conformer.

<sup>b)</sup> Conformational energies were computed using the GBMV calculations<sup>103</sup>. The conformational energy is the total energy of the oligomer including the 8 Aβ molecules and the copper ions. Standard deviation values are in parenthesis.